Study of low-head hydrostatic pressure water wheels for harnessing hydropower on small streams

Marco Licari*[1], Michel Benoit†[1], Fabien Anselmet‡[1], Vincent Kocher§[2], Simon Clément[2], and Pierre Le Faucheux[2]

[1]Aix Marseille Univ, CNRS, Ecole Centrale de Marseille, Institut de Recherche sur les Phénomènes Hors-Equilibre (IRPHE), UMR7342, 49 rue Frédéric Joliot-Curie, Technopôle de Château-Gombert, 13013 Marseille, France

[2]PYTHEAS Technology, 100 impasse des Houillères, ZA Le Pontet, 13590 Meyreuil, France

∗ Author's e-mail: marco.licari@mail.polimi.it
† Author's e-mail: benoit@irphe.univ-mrs.fr
‡ Author's e-mail: anselmet@irphe.univ-mrs.fr
§ Author's e-mail: vincent.kocher@pytheas-technology.com

Abstract

Due to the current concern for producing electrical power from renewable energy sources, there is a renewed interest in small size hydraulic turbines or wheels, operating on small streams with low head differences, such as the Hydrostatic Pressure Machine (HPM). Recently, a collaborative study between the research institute IRPHE and the PYTHEAS Technology company aims to understand the power production mechanisms involved in the HPM, its efficiency, and how the HPM's operation affects the hydraulic regime upstream and downstream of the HPM. An experimental research program is conducted in an hydraulic flume considering two scale models of HPM wheels with different shapes and characteristics. The experimental results (in particular power production and efficiency) are compared with predictions from semi-theoretical models adapted from existing modelling strategies. Overall, a good agreement is observed from the analyses performed within this study considering a range of hydraulic conditions (water discharge rate, upstream and downstream water levels). The results and performances of this type of wheel in terms of power and efficiency appear encouraging for application to real scale situations in rivers and streams. Indeed, the HPM results to be a promising device to simultaneously produce electrical power and control the water discharge.

Keywords: experimental hydraulics / hydroelectricity / hydraulic wheel / hydraulic energy / small hydropower / hydrostatic pressure machine

Nomenclature

Symbol	Definition	Units
bl	blade radial length, measured from the blade-hub attach to the blade tip	m
d_1	upstream free surface level	m
d_2	downstream free surface level	m
F_1	force due to the fluid pressure on the upstream side of the blade	N
F_2	force due to the fluid pressure on the downstream side of the blade	N
F_{bl}	force due to the fluid pressure on the blade	N
F_{hub}	force due to the fluid pressure on the wheel hub	N
F_{side}	force due to the fluid pressure on the machine lateral side	N
$F_{upstream}$	force due to the fluid pressure on the frontal upstream section	N
g	gravity acceleration	$m.s^{-2}$
H	hydrostatic head	m
H_{lost}	energy loss expressed as a loss of the available hydrostatic head	m
k	loss coefficient due to viscous power dissipation	-
L	axial length of the hydrostatic pressure machine	m
L_{ch}	width of the channel	m
P_{acc}	power loss due to the fluid acceleration	W
P_{exit}	power loss at the exit section due to partial ventilation	W
P_{id}	power of an ideal machine, with no energy loss	W
P_k	viscous power loss due to machine-fluid interactions	W
P_{meas}	power measured at the shaft by the instruments	W
P_{ni}	power of a non-ideal machine, with energy losses considered	W
P_{unvent}	power loss at the exit section due to perfectly unvented water cell	W
Q	volume flow rate	$m^3.s^{-1}$
Q_{max}	maximum volume flow rate dischargeable	$m^3.s^{-1}$
Q_{tot}	total volume flow accounting for both the processed water flow and leakage	$m^3.s^{-1}$
Q_{work}	working volume flow processed by the machine, without the leakage removed	$m^3.s^{-1}$
r_0	radius of the machine measured from the rotation center to the blade-hub attach	m
r_{mean}	radius of the machine measured from the rotation center to the blade mean height	m
r_{tip}	radius of the machine measured from the rotation center to the blade tip	m
S_{bl}	radial-axial surface of the blade	m^2
v_1	velocity of the upstream water flow	$m.s^{-1}$
v_2	velocity of the downstream water flow	$m.s^{-1}$
$v_{2,max}$	maximum velocity of the downstream water flow	$m.s^{-1}$
Z_{vent}	increase in elevation occurring in the cell before the fluid evacuation	m
α	empirical coefficient of partial ventilation	s^{-1}
Δh	free surface level drop due to the water flow acceleration	m
Δh_{max}	maximum free surface level drop due to the water flow acceleration	m
η_{av}	efficiency of the machine considering the available working volume flow rate	-
η_{tot}	efficiency of the machine considering the total volume flow rate	-
η_{vol}	volumetric efficiency	-
ρ	density of the fluid	$kg.m^{-3}$

φ	ventilation angle that determines the start of the cell emptying	*rad*
ω	angular velocity of the machine	$rad.s^{-1}$

Acronym	**definition**
EM	Electro-Magnetic
HPM	Hydrostatic Pressure Machine
IRPHE	Institut de Recherche sur les Phenomènes Hors Équilibre
M&C	Measure and Control
MRE	Mean Relative Error
RPM	Rounds Per Minute

1.Introduction: context and concept presentation

A renewed interest in hydroelectric plants of medium and small size has been demonstrated by the scientific and international community in the recent years (see, e.g., [1, 2, 3]), as these technologies are not only regarded as promising answers to cope with climate change impacts, but they could also unlock a huge hydraulic potential, currently unexploited. Considering European countries only, the estimated available sites account for *13 GW* of untapped hydraulic energy potential [2].

Various concepts of small hydraulic turbines are under research and optimisation process, and the "Hydrostatic Pressure Machine" (HPM) is the one considered in the present study [3], operating on sites with ultra-low hydraulic heads between *0.5 m* and *2 m*. The HPM concept, shown in *Figure 1*, derives from the hydraulic wheel, but has one peculiarity compared to the other hydraulic turbines. This machine, in fact, is not only an energy converter, but it could also be used as a water level regulation system: it can be installed in any river, but also in any irrigational canal, acting as a regulatory weir.

Figure 1. HPM under real field trial, developed by the HYLOW project, Bulgary (pictures taken from [1]).

Due to its design, the HPM converts the hydrostatic head created by the turbine itself: the difference between the upstream and downstream water levels applies a net pressure force on the machine blade in the same direction as the water flow, resulting in an applied torque on the machine shaft, thus converting hydraulic power into mechanical power.
In recent studies [3, 4, 5], various models have been proposed to explain the power conversion mechanism, but still no optimised HPM in terms of shape and dimensions has been proposed yet. The collaboration between the research institute IRPHE, specialized in fluid mechanics, and the PYTHEAS Technology company, developing energy conversion solutions for slow and intermittent energy sources, aims to deepen the knowledge of the power conversion mechanism and to study the effect of the geometry and shape of the HPM on its performances.
Two experimental scale models have been designed, built and tested in the "Herode channel", a testing facility available at the IRPHE, in Marseille. In this paper, the experimental results obtained are presented in terms of power, efficiency and performance predictions of the HPM. Thanks to these experimental campaigns, it can be assessed that the HPM is effectively a promising device both for power production and water level regulation purposes, while the collaboration between the two institutions is still undergoing, in order to produce more results soon.
The physical models developed are presented in Section 2, then the experimental set-up in the Herode flume is described in Section 3, as well as the design of the two tested scale models of the

HPM, along with their respective mechanical and electrical conversion chains. Their different conversion chains were designed to impose various working conditions on the wheels by using either an electromagnetic brake or a mechanical brake, simulating the presence of a power take-off system. Experimental results are presented and discussed in Section 4, before conclusions and perspectives are summarized in Section 5.

2. Physics and modelling of the Hydrostatic Pressure Machine

The most advanced model in the scientific literature seems to be the one proposed by Linton [5] following earlier works of Senior [4] and Senior *et al*. [3]. This model relies on several simplifying assumptions:

- steady state conditions (for the flow and motion of the wheel),
- the physics is bi-dimensional (and described in the vertical plane),
- there are no interactions between blades,
- blades are perpendicular to the water flux (as represented in *Figure 2*).
- upstream and downstream water levels d_1 and d_2 are constant, creating a nominal static head equal to the hub diameter $2r_0$.

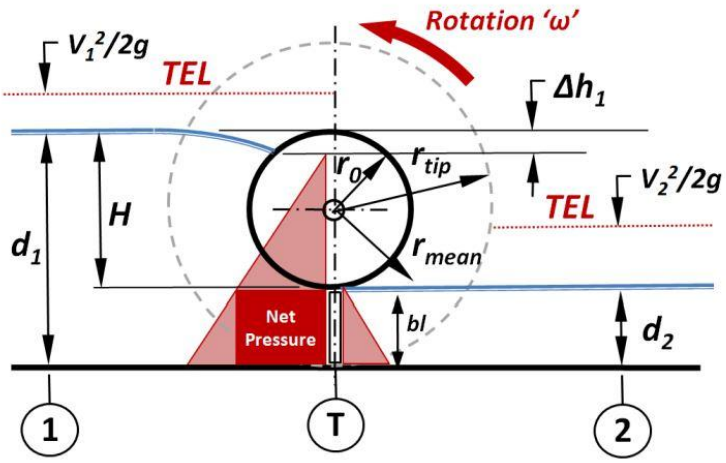

Figure 2. 2D scheme of an HPM under nominal operating conditions (reprinted from [5]).

2.1 HPM Ideal Model

The so-called "ideal model" does not consider any dissipative effect acting on the machine blades. Since the HPM is designed to convert mainly pressure energy, in this ideal approach, only pressure forces are considered. The net pressure force acting on the blade is expressed as:

$$F_p = F_1 - F_2 = \rho g(d_1 - d_2 - \Delta h)S_{bl} \quad (1)$$

where F_1 and F_2 are the resultant pressure forces on the blade on the upstream and downstream sides respectively. S_{bl} is the surface of the blade and, given that L is its width and bl is its radial length, it is estimated as follows:

$$S_{bl} = L\ bl \tag{2}$$

Δh is the drop in hydrostatic head due to the acceleration of the water flow, and it can be computed thanks to Bernoulli's theorem:

$$\Delta h = \frac{v_2^2 - v_1^2}{2g} \tag{3}$$

The acceleration of the water flow can be estimated thanks to the continuity equation:

$$Q = Ld_1v_1 = Ld_2v_2 \tag{4}$$

As the upstream water level is higher than the downstream one, the water flow is faster downstream than upstream (as a result of eq. (4)).
Another assumption made by Linton needs to be highlighted. Thanks to his experimental campaign, Linton observed a linear relationship between the wheel rotation velocity ω, and the water discharge passing through the HPM. Moreover, considering the operating conditions depicted in *Figure 2*, where the downstream water level rises up to the blade attach, Linton hypothesizes that the blades move at the same velocity as the downstream water velocity [5].
It is then possible to compute the ideal power as:

$$P_{id} = F_p v_{bl} = \rho g(d_1 - d_2 - \Delta h) S_{bl} v_2 \tag{5}$$

To calculate the efficiency of the machine, Linton only takes into account the hydrostatic head [5]:

$$\eta_{id} = \frac{P_{id}}{\rho g Q H} = \frac{P_{id}}{\rho g Q (d_1 - d_2)} \tag{6}$$

The normalized ideal results obtained using Linton's model are plotted in *Figure 3* and they are independent of the machine geometry.

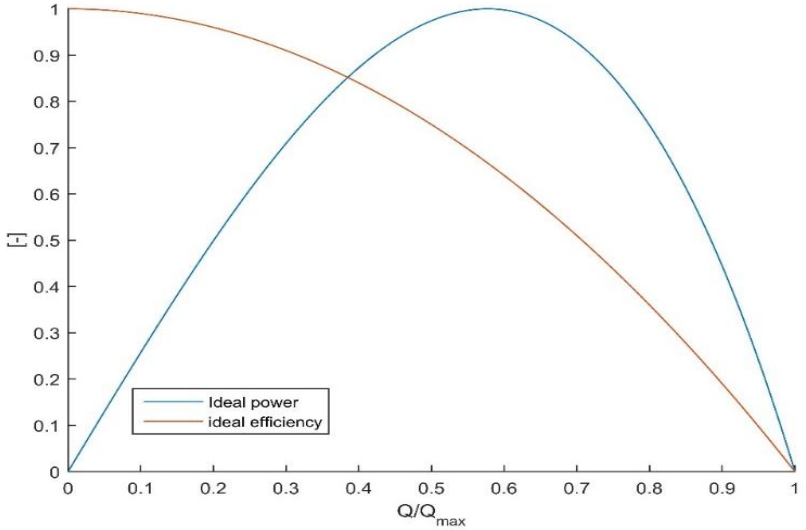

Figure 3. Power and efficiency of an HPM wheel based on the ideal model results, under nominal operating conditions.

In *Figure 3*, both the power and the water flow rate are normalized by their respective maximum values. While the maximum ideal power can be directly computed by maximising the power function relatively to the blade velocity, more considerations are needed for the definition of the maximum water flow dischargeable by the HPM.
The operational limit of the machine occurs when all the hydrostatic head available is converted into dynamic head:

$$\Delta h_{max} = d_1 - d_2 \tag{7}$$

In this condition, the net pressure force acting on the blade disappears, and no power is produced, as it can be verified applying eq. (7) to eq. (1) and to eq. (5). When this operational boundary is reached, the HPM rotates at its maximum angular speed, and the maximum discharged flow rate can be computed considering eq. (3), eq. (4) and eq. (7):

$$v_{2,max} = \sqrt{\frac{2g(d_1 - d_2)}{1 - \left(\frac{d_2}{d_1}\right)^2}} \tag{8}$$

$$Q_{max} = L d_2 v_{2,max} \tag{9}$$

2.2 More realistic (non-ideal) models

Although the ideal model allows a first assessment of the HPM operation and performances, various phenomena occur under real operating conditions, reducing the power effectively obtainable by the hydraulic machine. Some of these effects are discussed below, and expressions are proposed to be incorporated in more realistic versions of the HPM model.

2.2.1 Blade-fluid interaction losses

First, power losses due to viscosity are an inevitable consequence of the blade-fluid turbulent interaction. The following semi-empirical function is proposed for the estimation of these losses:

$$P_{k,1} = k_1 \, \rho g Q H_{lost} \tag{10}$$

$$H_{lost} = \frac{(v_2 - v_1)^2}{2g} \tag{11}$$

Alternatively, a second formulation can be used to estimate the losses due to the blade-fluid interaction, expressed as follows:

$$P_{k,2} = \frac{1}{2} \rho k_2 L b l v_{bl}^3 \tag{12}$$

The dimensionless coefficients k_i in eq. (10) and eq. (12) are determined experimentally, allowing to express a first definition for the non-ideal power:

$$P_{ni} = P_{id} - P_{k,1} \tag{13}$$

The eq. (13) computes the maximum hydraulic power convertible by the HPM under the non-ideal condition of power losses due to the blade-fluid turbulent interaction.

2.2.2 Ventilation losses

This phenomenon occurs at the exit of the wheel blade from water during the emptying mechanism of the water volume delimited between two blades (the so called "cells").
Assuming cells are fully filled with water until reaching the atmosphere, power at the exit of the wheel is estimated by applying the momentum equation at the exit of the wheel:

$$P_{exit} = Q^3 \rho \frac{\frac{bl}{d_2} - 1}{(Lbl)^2} + \frac{1}{2} \rho g Q \frac{{d_2}^2 - bl^2}{bl} \tag{14}$$

However, this involves that an important volume of water is lifted until the water free surface. In reality, air starts replacing the water long before the surface. Assuming that air can freely fill the cell from the angle φ, the power is adjusted as follows:

$$P_{unvent} = P_{exit} + \frac{\rho g Q}{2L} Z_{vent}(Z_{vent} - 2L) \tag{15}$$

$$\mathrm{Z_{vent}} = \mathrm{r_{mean}}(1 - \cos \varphi) \tag{16}$$

Currently, eq. (15) largely over-estimates losses as air filling is restrained. A coefficient α is then introduced to estimate the rate of the cell filling. Finally, it is possible to compute the power lost at the exit section of the machine due to the cell ventilation losses as follows:

$$P_{exit} = (1 - \alpha \frac{\varphi}{\omega}) P_{unvent} \tag{17}$$

For the sake of clarity, it is here highlighted that the empirical coefficient α is not dimensionless but, has a unit of s^{-1}. Therefore, scaling laws need to be applied if it is needed to compare α obtained by different experiments.

2.2.3 Acceleration losses

Acceleration losses are calculated by applying the momentum equation on the upstream part of the fluid domain:

$$P_{acc} = r_{mean}\omega \left\{F_{hub} + F_{bl} + F_{side} - F_{upstream} + Q\rho v_{bl}\left(1 - \frac{blL}{d1L_{ch}}\right)\right\} \quad (18)$$

where F_{hub}, F_{bl}, F_{side} and $F_{upstream}$ are the respective pressure forces.

2.2.4 Flow leakage

Another negative effect concerning the power production is the presence of by-passed water flow during operation. The totality of the by-passed flow is due to the gap between the fixed and rotating components of the HPM. In order to avoid mechanical friction, these gaps are needed between the hydraulic wheel and the lateral walls, as well as between the wheel and the channel floor. While the lateral gaps have constant dimensions, a bigger portion of the flow is able to by-pass the wheel underneath the blade whenever the blade is not perpendicular to the channel floor.
The processed flow Q_{work}, considering the operating conditions depicted in *Figure 2*, can be analytically estimated given that the wheel angular velocity and the velocity profile of the water flow at section *T* are known:

$$Q_{work} = \int_{r_0}^{r_{tip}} v(r)\, dr = \int_{r_0}^{r_{tip}} \omega r L\, dr = \omega r_{mean} L bl \quad (19)$$

The geometrical constant r_{mean} is the radius of the rotor at the mean blade height:

$$r_{mean} = r_0 + \frac{bl}{2} \quad (20)$$

As discussed in the experimental results presentation (see Section 4 hereafter), flow leakage appears to be mainly driven by the increase of the water level difference and, as for the blade-fluid interaction losses (see Sub-section 2.2.1), leakage losses will be experimentally estimated.

2.3 Definition of the machine efficiency

Various efficiencies are defined to properly characterise the HPM ability to convert hydraulic power. While the total efficiency η_{tot} is computed on the total water flow rate and evaluates the global performance, the available efficiency η_{av} considering only the net processed flow rate only accounts for the hydrodynamics quality of the HPM:

$$\eta_{tot} = \frac{P_{ni}}{\rho g Q_{tot} H} \quad (21)$$

$$\eta_{av} = \frac{P_{ni}}{\rho g Q_{work} H} \quad (22)$$

Furthermore, it is convenient to define the volumetric efficiency as the ratio between the effectively processed water flow rate and the total water flow rate:

$$\eta_{vol} = \frac{Q_{work}}{Q_{tot}} \tag{23}$$

Doing so, the volumetric efficiency allows to better evaluate the leakage's influence on the HPM performance, being the volumetric efficiency related to the hydrodynamic quality and global quality of the machine as follows:

$$\eta_{tot} = \eta_{vol}\eta_{av} \tag{24}$$

It is finally possible to define the technical efficiency, as the efficiency considering the full set of power losses and computing the full technical performance of the machine:

$$\eta_{th} = \frac{P_{id} - P_{k,2} - P_{acc} - P_{exit}}{\rho g Q_{tot} H} \tag{25}$$

3. Experimental set-up

Two different scale models of HPM have been tested in the "Herode Channel", a pre-existing experimental facility located in the research institute IRPHE, in Marseille. The two experimental scale models have different geometries and they have been designed to study the HPM under various operating conditions. The concepts behind these two machines are discussed in Sub-sections 3.2 and 3.3, while the Herode Channel is first presented in Sub-section 3.1.

3.1 The Herode hydraulic channel

In *Figure 4*, a schematic view of the Herode channel is given. This testing facility is divided in two main areas: the free-surface zone with a rectangular cross-section, that corresponds to the actual testing environment, and the recirculation pipe located below.

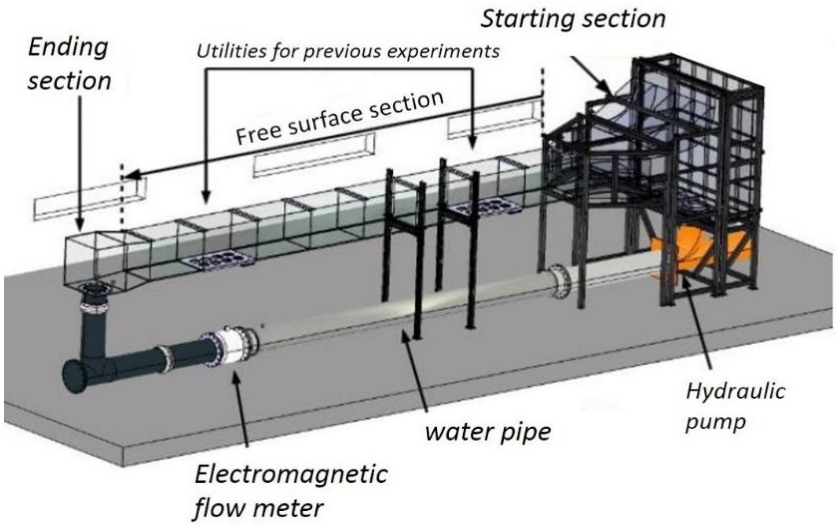

Figure 4. Schematic view of the Herode channel at IRPHE.

The total water volume present in the channel can be regulated by a secondary system of charging and discharging conducts, allowing to directly control the free-surface level. Whenever a physical

barrier of any kind is installed in the channel and the pump is running, the upstream and downstream free-surface levels cannot be directly fixed nor modified due to the lack of regulatory weir (as the total volume of water circulating in the flume is fixed for a given test).
In the testing section, the free-surface level can reach up to *0.55 m* and the internal width of the channel is of *0.62 m*, while the total length of the testing section is *8 m*.
The water flow rate is measured using an electromagnetic flow meter, while a hydraulic pump allows the operator to adapt the water discharge to the chosen testing conditions.

3.2 The IRPHE experimental HPM scale model

A first HPM scale model was built at IRPHE using a simple geometry for the blades (*Figure 5*). It consists in a 12 blades rotor, where a transmission belt conveys the mechanical power to the measure and control ("M&C") system, located well above the water surface.
The 12 blades of the hydraulic wheel have a *2 mm* thickness, a radial length of *185 mm* and they span the hub axial length of *488 mm*. The central hub shape is a dodecagonal prism, *488 mm* of width and a dodecagon circumferential radius of *145 mm*.

Figure 5. IRPHE HPM wheel operating in the Herode Channel.
The water flows from the left and the wheel is rotating counterclockwise.

The transmission system is composed of a toothed transmission belt, *16 mm* wide, which connects the "motor" gear mounted on the wheel shaft, to the "transmission" gear, mounted on the M&C system. The motor gear has *84* teeth and the transmission gear *14*, so the angular speed of the M&C shaft is 6 times the motor shaft angular speed. This transmission ratio has been chosen to respect various electrical and mechanical limits concerning the M&C system and is related to the expected HPM operating conditions in terms of torque and angular speed.
Regarding the M&C system represented in *Figure 6*, the measurement system features a dynamic torque transducer (T22/10Nm made by HBM) and a RVDT angular position sensor (R30D by TE Connectivity ltd.). Two brakes have been selected for applying the mechanical load to the transmission shaft, a mechanical band brake and an electro-magnetic (EM) brake. The mechanical brake has been designed, built and assembled by IRPHE and it is adjustable manually thanks to a regulation screw. The EM brake was bought (model FRAT 120 by Merobel), it is remotely controllable by altering the incoming excitation current and it applies a constant resistive torque independent from the angular speed.

The hydraulic wheel, the transmission system and the M&C system have been mounted in a PMMA supporting structure, so that it is possible to position and fix the HPM without modifying the pre-existing testing facility.

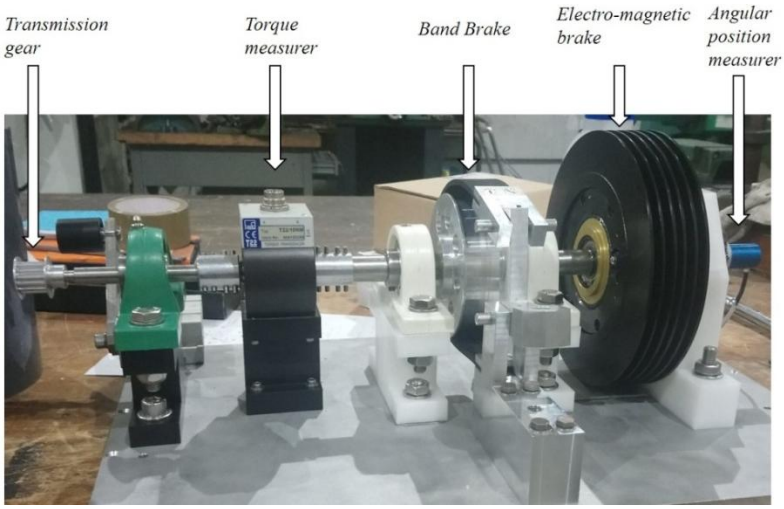

Figure 6. Measurement and control system of the IRPHE experimental HPM model.

3.3 PYTHEAS Technology experimental HPM scale model

For the PYTHEAS Technology experimental HPM model, two parts were designed: the HPM wheel and a shroud. The hydraulic wheel is designed with 12 blades attached to a central hub. Blades are as long as the diameter of the central hub. To minimize turbulence each time a blade enters the free surface, they present an entry angle of *30°*, and the twisted shape not only improves the blade cell emptying but also prevents air to be sucked in at the entrance.

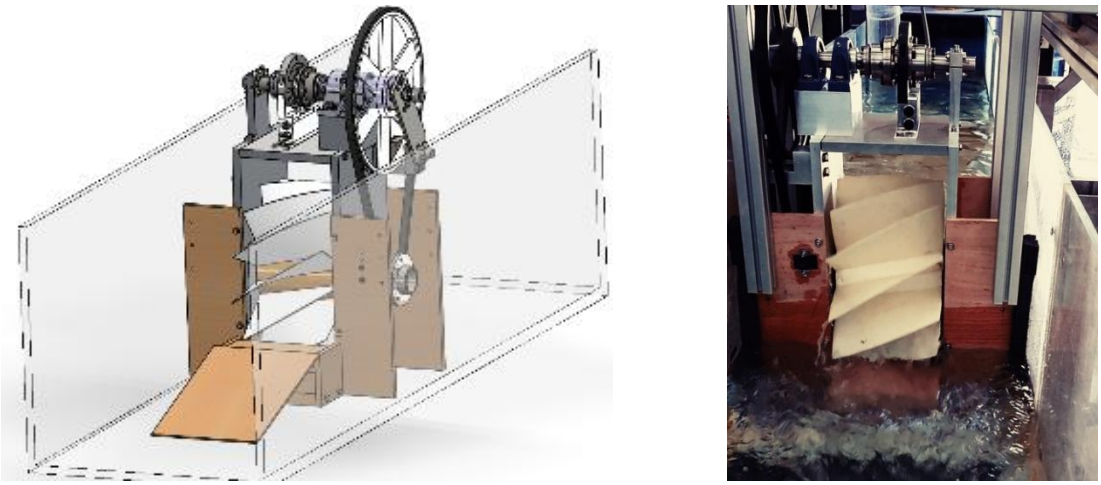

Figure 7. Model views of the PYTHEAS experimental system
(left: drawing of the wheel and M&C system ; right: picture of the wheel operating in the flume)

The second main element of the system is the shroud. It consists of an adaptation of the channel floor to ensure efficient compression during the wheel cycle and to reduce the by-passed flow underneath the wheel blades, as depicted in *Figure 8*. Various shroud configurations have been tested: the covered angle between the vertical and the entrance or exit section could be of *40°* or *56°*, as shown in *Figure 8*.

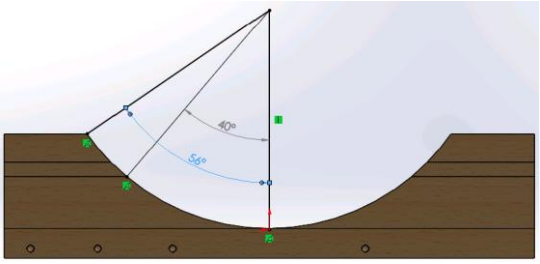

Figure 8. Shroud design of PYTHEAS HPM scale model

To optimise the filling and emptying of the cells, the wheel should be smaller than the complete inner width of the channel where the HPM is installed. According to [6], the gap between the wheel sides and the channel lateral walls must be at least equal to half of the wheel's width, especially on the downstream part where the water needs to be quickly discharged. This is the reason why the wheel axial length is *238 mm*, the blade radial length is *150 mm* while the hub diameter is *150 mm*.
Like for the IRPHE HPM model, rotational speed and torque are measured on a shaft above the free surface: an encoder ERN 1020 from Heidenhain is used to measure the angular velocity and a torque transducerT40S2 (range *0-100N.m*) from HBM for the torque.
The resistive torque is applied with a mechanical brake, manually adjustable thanks to two plates tightened by screws on the transmission shaft. Basically, the measure and control system set-up of the PYTHEAS Technology and IRPHE HPM wheels share the same concept, with the only difference of a second electromagnetic brake installed on the IRPHE transmission shaft.

4. Analysis of experimental results

4.1 General considerations on experimental protocol

The results in terms of converted power and related efficiency are disclosed hereafter, both for the IRPHE and the PYTHEAS HPM wheels.
Furthermore, it has to be highlighted that the PYTHEAS HPM operated under Linton's nominal conditions of constant downstream and upstream water levels: the downstream surface rises up to the lowest point on the hub, while the upstream water level reaches the highest point on the hub circumference (as depicted in *Figure 2*). Since the hydraulic system response to a higher mechanical load imposed to the HPM is a wider difference between the upstream and downstream levels, both Senior's [4] and PYTHEAS experiments relied on a system of either adjustable or fixed weirs and variation of the total water volume available in the testing channel for exogenously fixing the free-surface levels at the protocol values.
In order to study a wider range of operating conditions, the IRPHE experimental campaign did not operate under constant water levels: for a higher mechanical load imposed on the HPM, the upstream and downstream water levels were free to adapt themselves at the hydraulic system equilibrium.
These two approaches have been chosen for better understanding the HPM physics, since this hydraulic machine is studied not only as an energy converter but also as a water level regulation system. Previous experiments in the scientific literature [5] already demonstrated how, during real field tests, the assumption of constant water levels is not always granted, so further investigation on the relation between the machine mechanical load and the free-surface levels was considered useful and justified the two chosen complementary approaches.

Five distinct parameters are measured during the experimental campaigns:

- Two hydrostatic probes measure the upstream and downstream water levels. Incertitude on these measurements is about *1 mm*.
- As explained in the scale models descriptions, encoders measure the angular velocity and torque transducers measure the applied resistive torque.
- The total water flow discharged from the testing section is measured on the exit pipe. Doing so, the measured flow rate corresponds to the total flow rate streaming in the free-surface section, accounting for both the water flux effectively processed by the HPM and the by-passed water flow.

4.2 Experimental results obtained with the IRPHE wheel

Since the water heights are not constant for the experiments with IRPHE wheel, the number of free variables increases compared to Linton's model. More specifically, there are three variable parameters for the IRPHE experiments: the resulting torque and the angular velocity of the HPM, which can be studied imposing different mechanical loads and water flow rates, while the water levels difference represents the third variable. Thanks to the conducted experimental campaign, empirical observations suggested that the difference between the upstream and downstream water levels is directly related to the total water volume available in the testing channel: setting the HPM torque and angular speed at the same values produced the same upstream and downstream water heights and difference only if the same water volume was present.
From this observation, the following experimental protocol was developed: *4* different initial water volumes were tested, and for each water volume *4* angular velocities were studied, increasing progressively the mechanical load. *82* different equilibrium points have been collected, and it is possible to observe the related power and efficiency curves in *Figures 9, 10* and *11*.
All the variables are plotted as functions of the hydrostatic head difference $d_1 - d_2$, while the curves are parameterized for a fixed motor-shaft RPM. Considering the plotted results, the amount of water volume available in the channel is conveniently expressed by the term h_z, the homogenous water height when the channel is completely at rest. Moreover, for the sake of clarity, only the results for h_z at *25 cm* are plotted here, while the qualitative comments on this case hold across all the IRPHE results.

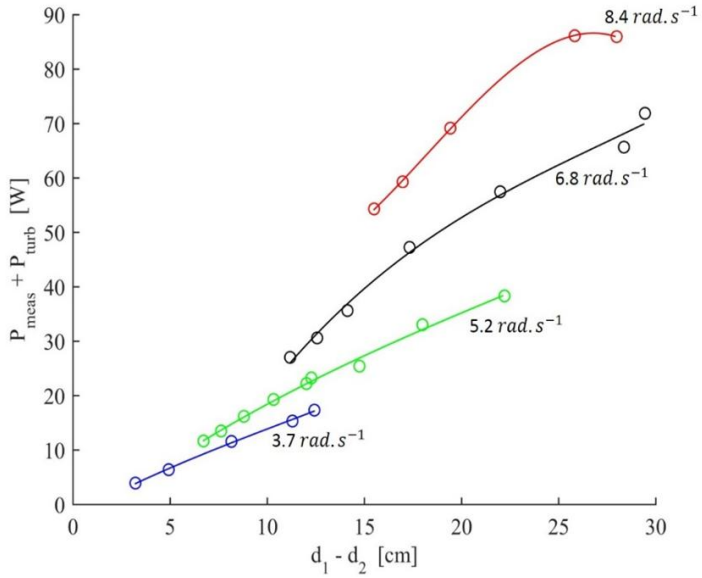

Figure 9. Experimental ideal power for various fixed angular velocities (IRPHE wheel)

Starting with the results in *Figure 9*, the experimental ideal power $P_{meas} + P_k$ increases for higher static head and higher RPM, in accordance with the power formalisation expressed in eq. (5). Given the relatively low values of RPM studied, the nonlinear effects of static head drop affecting the obtained power and expressed by eq. (3) were slightly appreciable, explaining the linear slope of the curves at $3.7\ rad.s^{-1}$, $5.2\ rad.s^{-1}$ and $6.8\ rad.s^{-1}$, while for the fastest RPM curve, due to faster flow velocities involved, nonlinear effects were more appreciable. Furthermore, the power curves show already that, for an ideal machine, the HPM can convert up to *172 W* per meter of width, given a very low hydrostatic head of *25 cm*. The results in terms of efficiency seem promising as well.

As shown in *Figure 10*, unlike the power curves, the efficiency curves drop for higher RPM: the effect is due to the viscous effects for the blade-fluid interactions. Eq. (10) and eq. (11) show the relation between the power losses and the blade velocity: as the HPM is rotating faster, higher blade velocities cause higher turbulent power dissipation. Furthermore, it can be noticed that the gap between total and available efficiency increases as the static head difference increases. This effect can be explained considering eq. (24): the water leakage increases with the upstream and downstream water level difference. Consequently the volumetric efficiency drops, widening the gap between available and total efficiency.

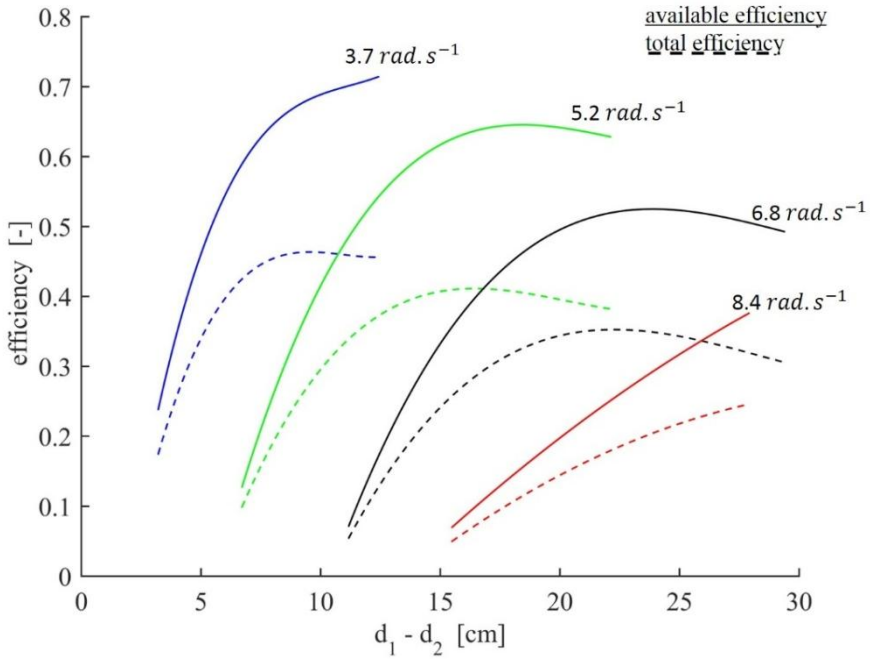

Figure 10. Available and total efficiency compared for different fixed angular velocities (IRPHE wheel)

Finally, as shown in *Figure 11*, it is possible to compare the obtained results in terms of experimental ideal power $P_{meas} + P_k$ and the theoretical ideal power P_{id}. The mean relative error (MRE) between the experimental and theoretical powers for all the *82* studied conditions results to be lower than *10%*, computed as follows:

$$MRE = \sum_{i=1}^{82} \frac{P_{id,i} - (P_{meas} + P_k)_i}{P_{id,i}} = 9.76\% \tag{26}$$

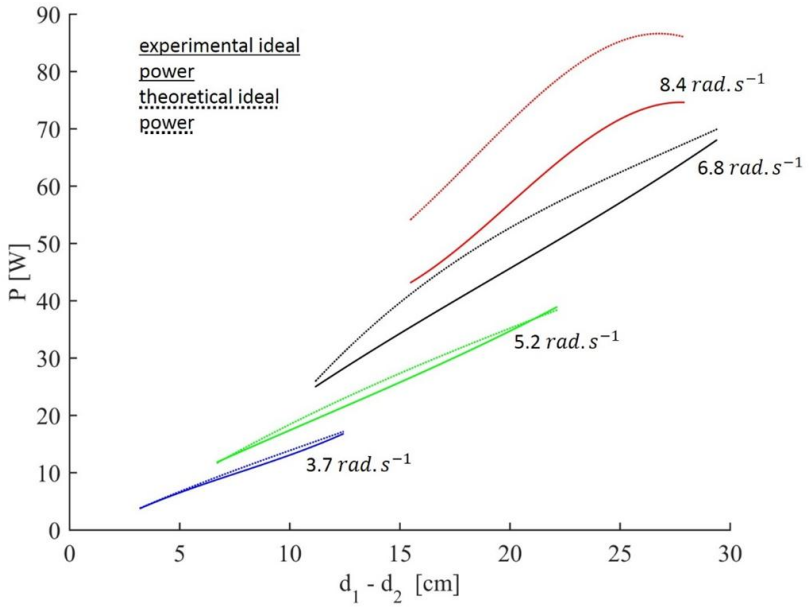

Figure 11. Comparison of experimental ideal power and theoretical ideal power (IRPHE wheel)

4.3 Experimental results obtained with the PYTHEAS Technology wheel

For the experimental protocol adopted for the PYTHEAS experiments, it must be considered that, as explained in Sub-sections 3.1 and 3.2, the testing channel operates as a closed loop. At the beginning of the tests, with the pump running, the operator sets the upstream water level at the chosen nominal value of *31.5 cm* while, at the same time, the resistive torque is set at its maximum. Then, the operator increases the pump power and reduces the breaking torque to keep the upstream water level constant and record data for various flow rate and mechanical load conditions. Given the initial presence of enough water in the channel, it was possible to fix the downstream water level at the nominal value of *16.7 cm*. The nominal head difference is then *14.8 cm* and is constant all along the studied power curve conditions.

Figure 12 shows the power curves obtained with two shroud conditions. The red curve corresponds to a *40°* downstream shroud, the blue one is set with a downstream shroud angle of *56°*, while the upstream shroud angle is kept constant at *56°* for both tests. The gap between the two curves can be explained by the ventilation phenomenon, as formalized by eq. (14) and eq. (15). With the tallest shroud, the water remains in the cell for a longer time: an effort from the wheel is then required to rise this volume before air fills it, creating additional losses.

However, an optimum design should be reached. Due to the twisted and oblique shape of the blades, the downstream shroud should be designed containing at least an entire blade, but a shorter shroud could bring new other losses. During the compression phase, in fact, a shorter shroud would cause the water to be depressurized before the whole volume crosses the vertical line. For the current experiment, the optimal trade-off angle is estimated around *30°*.

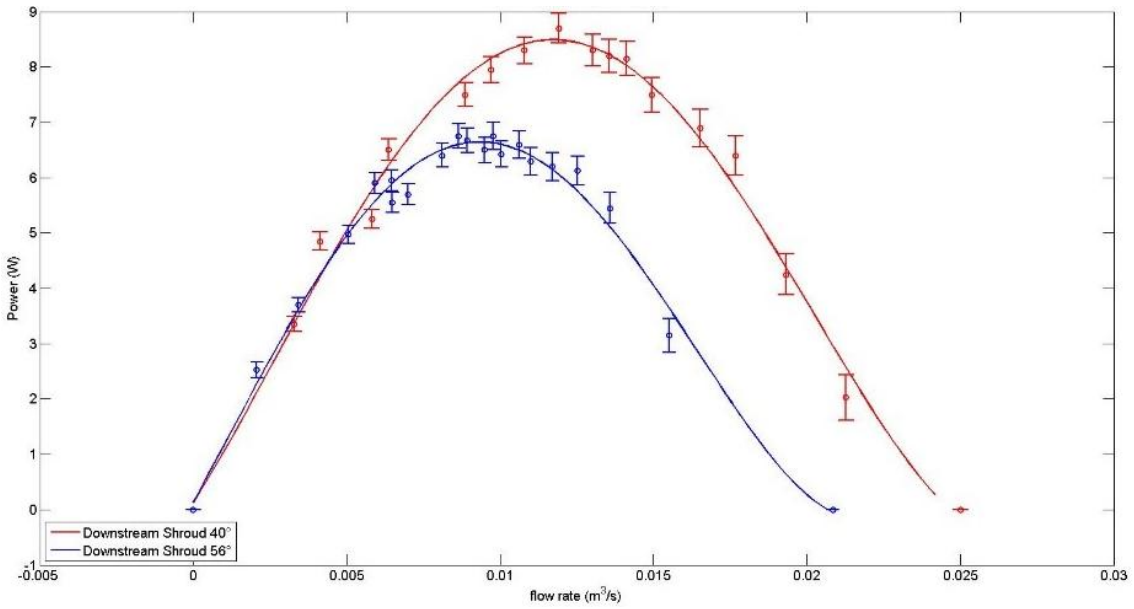

Figure 12. Converted power for two downstream shroud configurations (PYTHEAS wheel)

Figure 13 shows the corresponding technical efficiencies. In both configurations, efficiency is nearly linear with the flow rate. It can be seen that efficiency is lower with the *56°* shroud, which matches the observations made from the power curves in *Figure 12.*

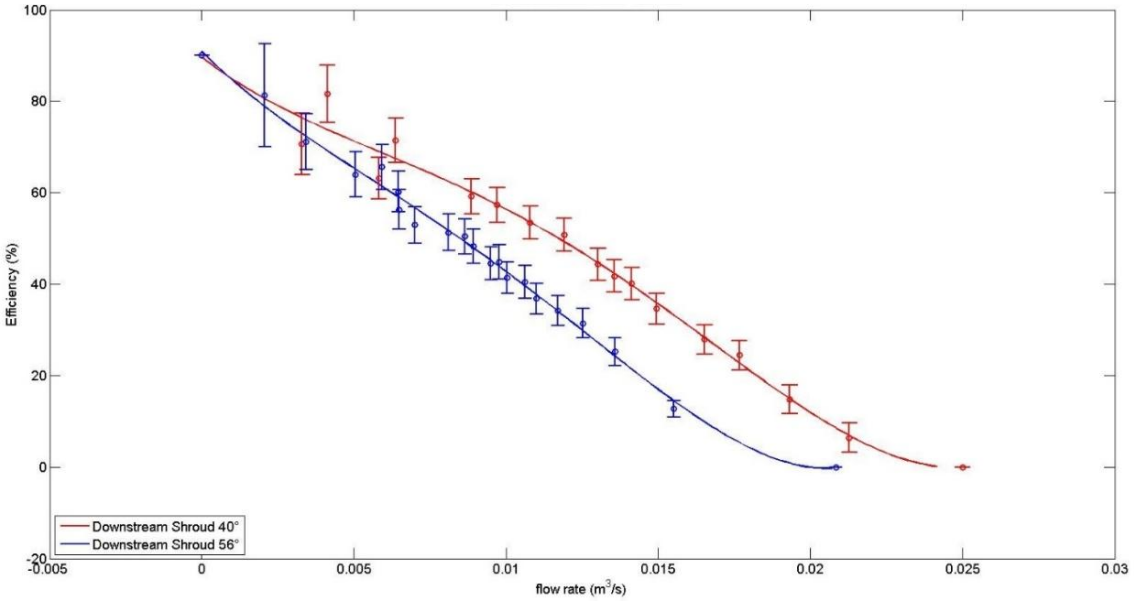

Figure 13. Technical efficiency η_{th} (eq. (25)) for two downstream shroud configurations (PYTHEAS wheel)

Figure 14 compares experimental results, with their best fit and error bars, with the power and efficiency estimated with the analytical model described in Sub-sections 2.2 and 2.3. The experimental data set was measured with an upstream and downstream shroud of *40°* and an upstream water level set at *33 cm*. The descending curves represent the global technical efficiencies (see eq. (25)), while the parabolic curves represent the converted power. All losses (acceleration, turbulence and ventilation) are applied in the model. As said previously, empirical coefficients C_t, φ and α are respectively set to *5.2*, *30°* and *0.8* s^{-1}.

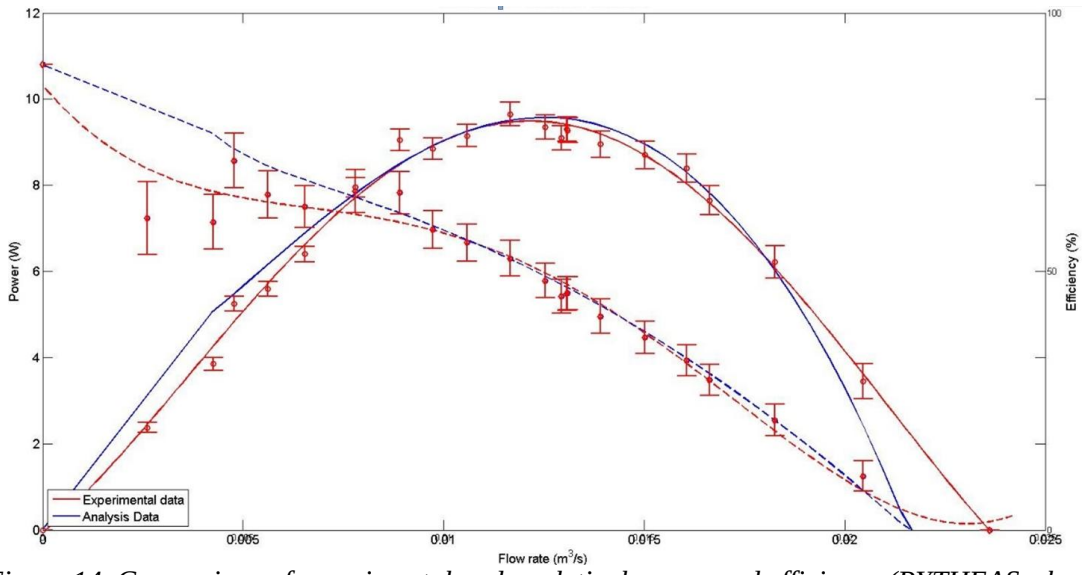

Figure 14. Comparison of experimental and analytical power and efficiency (PYTHEAS wheel)

In this configuration, both data sets are close. The maximum difference (*12%*) appears for small flow rates. As ventilation power largely over-estimates losses for low rotation velocities, it is neglected in this area. In the range where the turbine is used, power differences are below *4.5%*.
The analytical model's efficiency results are within the incertitude of the experiments. Less than *2.5%* deviation is observed for flow rates above *0.0056* $m^3.s^{-1}$. This accurate correlation between the analytical and experimental datasets will allow to extrapolate data for different geometries. As expected, the peak of power and efficiency does not always match, but the model still appears to explain reasonably well the power prediction and the main sources of losses.
Finally, *Figure 15* shows the flow rate as a function of the rotational velocity. As expected, the flow rate through the turbine is nearly linear with its rotation speed. Color on test data is function of the head loss. A small variation occurs at high flow rates where fluid is not homogenous anymore. A significant amount of air is observed in the cell, reducing the flow rate through the wheel.

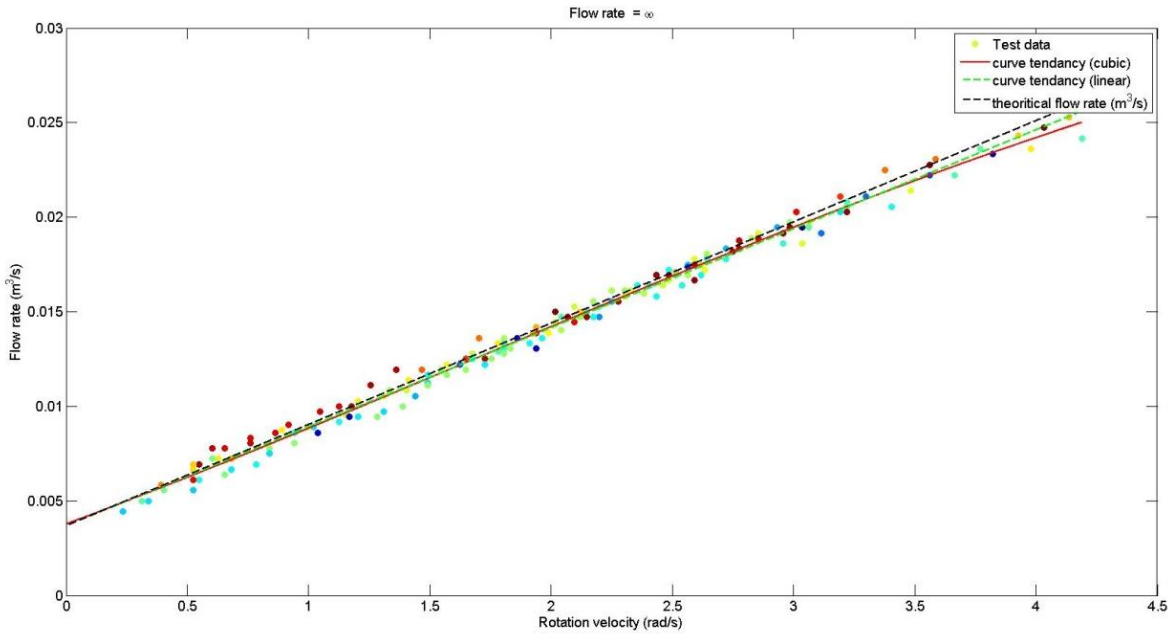

Figure 15. Variation of flow rate as a function of the rotation velocity (PYTHEAS wheel).

5. Conclusions and perspectives

The tests performed in this study show a very good agreement between the analytical models and the experimental results, by adding just a few semi-empirical models describing non-ideal effects, with empirical coefficients determined from experimental measurements. Based on these reliable results, estimation of the power production and efficiency for a site of any scale can be assessed.
These tests also permitted to identify the hydrodynamic behavior of the wheel, especially how changing the breaking torque (representing the power take-off system) and the water level impacts the behavior of the HPM. Possible improvements of the wheel (geometry, dimensions, shape of the blades, etc.) and the shroud were identified, which will be tested in the next steps of the project.
The optimal operating point in flow rate, or equivalently in rotation speed, confirms the relevance and benefit of the HPM wheel. This type of turbine appears as one of the most suitable solutions to efficiently harvest energy from such small hydrostatic head difference.
The next steps of the project will address: i) a dedicated study to improve the performances of the wheel, ii) the adaptation of the generator that converts the slow motion of the wheel into electricity, and iii) the elaboration of the control law of the wheel. In fact, another advantage of this wheel is the linear relation between flow rate and rotational speed. This relation makes the wheel also useful for flow rate control. By adjusting the rotation speed of the wheel, we can control the flow rate and produce power simultaneously: this is no less than an hydraulic regulation work harvesting energy.

6. Acknowledgements

M. Benoit and F. Anselmet thank the board of IRPHE lab. for funding the experimental program on the IRPHE wheel and the 6-month internship scolarship of M. Licari.

7. References

[1] European Commission, HYLOW project: Development of hydropower converters with very low head differences. European project number 212423 funded under the Framework Program 7 – Energy 2007 (FP7-Energy-2007-1-RTD), 2008-2013. (http://www.hylow.eu/)

[2] O. Paish, Small hydro power: technology and current status, Renew. Sustain. Energy Rev. 6(6), 2002, 537-556.

[3] J. Senior, N. Saenger, G. Müller, New hydropower converters for very low-head differences. J. Hyd. Res., 48(6), 2010, 703-714.

[4] J.A. Senior, Hydrostatic pressure converters for the exploitation of very low head hydropower potential, PhD thesis of the University of Southampton (UK), 2009.

[5] N.P. Linton, Field trials and development of a hydrostatic pressure machine, PhD of the University of Southampton (UK), 2013.

[6] S. Paudel, Experimental and numerical study of Dethridge Wheel for pico-scale hydropower generation, PhD of Darmstadt University (Germany), 2015.